Three Conformational States of the p300 CH1 Domain Define Its Functional Properties†

Ravina Dial,‡ Zhen-Yu J. Sun,§ and Steven J. Freedman*,‡,||

Division of Hemostasis and Thrombosis and Division of Hematology-Oncology, Beth Israel Deaconess Medical Center, 330 Brookline Avenue, Boston, Massachusetts 02215, and Department of Biological Chemistry and Molecular Pharmacology, Harvard Medical School, 240 Longwood Avenue, Boston, Massachusetts 02115

Received June 10, 2003; Revised Manuscript Received June 25, 2003

ABSTRACT: Numerous transcription factors interact with the basal transcriptional machinery through the transcriptional co-activators p300 and CREB-binding protein (CBP). The Zn^{2+}-binding cysteine/histidine-rich 1 (CH1) domain of p300/CBP binds many of these transcription factors, including hypoxia-inducible factor (HIF). We studied the structural and biophysical properties of the p300 CH1 domain alone and bound to the HIF-1α C-terminal transactivation domain (TAD) to understand the diverse binding properties of CH1. The Zn^{2+}-bound CH1 domain (CH1−Zn^{2+}) and the HIF-1α TAD−CH1 complex (CH1−Zn^{2+}−HIF-1α) are similarly helical, whereas metal-free CH1 is mostly random coil. CH1−Zn^{2+} undergoes noncooperative thermal denaturation, does not have a near-UV elliptical signal, and binds the hydrophobic fluorophore ANS. In contrast, the CH1−Zn^{2+}−HIF-1α complex undergoes cooperative thermal denaturation, does produce a near-UV signal, and does not bind ANS. Addition of Zn^{2+} ions to metal-free CH1 produced one conformational change, and subsequent addition of a HIF-1α TAD peptide induced a second conformational change as detected by intrinsic tryptophan fluorescence spectroscopy. The NMR $^{1}H-^{15}N$ HSQC spectrum of CH1−Zn^{2+} exhibits few poorly dispersed peaks with broad line widths. Removal of metal ions produces more poorly dispersed peaks with sharper line widths. Addition of a HIF-1α TAD peptide to CH1−Zn^{2+} produces many well-dispersed peaks with sharp line widths. Taken together, these data support three conformational states for CH1, including an unstructured metal-free domain, a partially structured Zn^{2+}-bound domain with molten globule characteristics, and a stable, well-ordered HIF-1α TAD−CH1 complex.

Transcriptional activation requires the coordinated assembly of large protein complexes at gene promoters (*1*). Essential components of these transcriptosomes include a transcription factor, one or more transcriptional co-activators, and the basal transcriptional machinery, including RNA polymerase. General transcriptional co-activators belonging to the p300/CBP[1] family serve as adapters between a multitude of transcription factors and the basal transcriptional machinery. In addition, they facilitate transcription by opening chromatin through their intrinsic histone acetyltransferase activity. Recently, p300 was shown to have ubiquitin ligase activity used to target p53 for degradation (*2*). Consequently, p300/CBP has diverse roles in cell growth, differentiation, transformation, and apoptosis (*3*, *4*). Deficiencies of p300 and CBP result in developmental disorders in animals and humans; the human disease Rubinstein-Taybi syndrome is caused by heterozygosity for CBP gene mutations (*5*). In addition, chromosomal translocations in some hematological malignancies produce fusions of p300/CBP with other proteins (*6*).

CBP and p300 are paralogous proteins containing multiple protein interaction domains (Figure 1A), some of which can bind numerous transcription factors (*7*−*9*). Many of these transcription factors bind to the Zn^{2+}-binding cysteine/histidine-rich domains, CH1 and CH3 [also termed TAZ1 and TAZ2 (*10*), respectively]. Remarkably, the 100-residue CH1 and CH3 domains are approximately 30% identical, yet they bind nearly distinct sets of transcription factors. For instance, CH1 binds HIF-1α, CITED2, Stat2, p53, MDM2, NFκB, Ets-1, and others (*11*−*16*). Of these transcription factors, CH3 binds only Ets-1 and p53; however, different regions of p53 interact with CH1 and CH3 (*14*, *17*). Therefore, important questions about p300/CBP function relate to the diverse yet specific binding properties of CH1 and CH3. CH2 is also a Zn^{2+}-binding domain but is

† This work was supported by an NIH K08 award from the NHLBI and by an ASH Scholar Award from the American Society of Hematology to S.J.F.

* To whom correspondence should be addressed. E-mail: sjf@massmed.org. Telephone: (484) 344-3770.

‡ Beth Israel Deaconess Medical Center.

§ Harvard Medical School.

|| Present address: Merck Research Labs, Department of Clinical Pharmacology/Experimental Medicine, 5 W. Sentry Parkway, Blue Bell, PA 19422.

[1] Abbreviations: HIF, hypoxia-inducible factor; CREB, cAMP response element-binding protein; CBP, CREB-binding protein; CITED2, CBP/p300 interacting transactivator with an E (glutamic acid)/D (aspartic acid)-rich tail 2; αLA, α-lactalbumin; TAD, transactivation domain; CH1−3, cysteine/histidine-rich domains 1−3, respectively; CH1−Zn^{2+}, Zn^{2+}-bound CH1; CH1−Zn^{2+}−HIF-1α, HIF-1α-bound CH1−Zn^{2+}; PHD, plant homeodomain; NMR, nuclear magnetic resonance; CD, circular dichroism; HPLC, high-pressure liquid chromatography; SDS−PAGE, sodium dodecyl sulfate−polyacrylamide gel electrophoresis; IPTG, isopropyl β-D-thiogalactopyranoside; ANS, 1-anilinonaphthalene-8-sulfonic acid; rmsd, root-mean-square deviation; EC_{50}, 50% effective concentration.

10.1021/bi034989o CCC: $25.00
Published on Web 07/30/2003

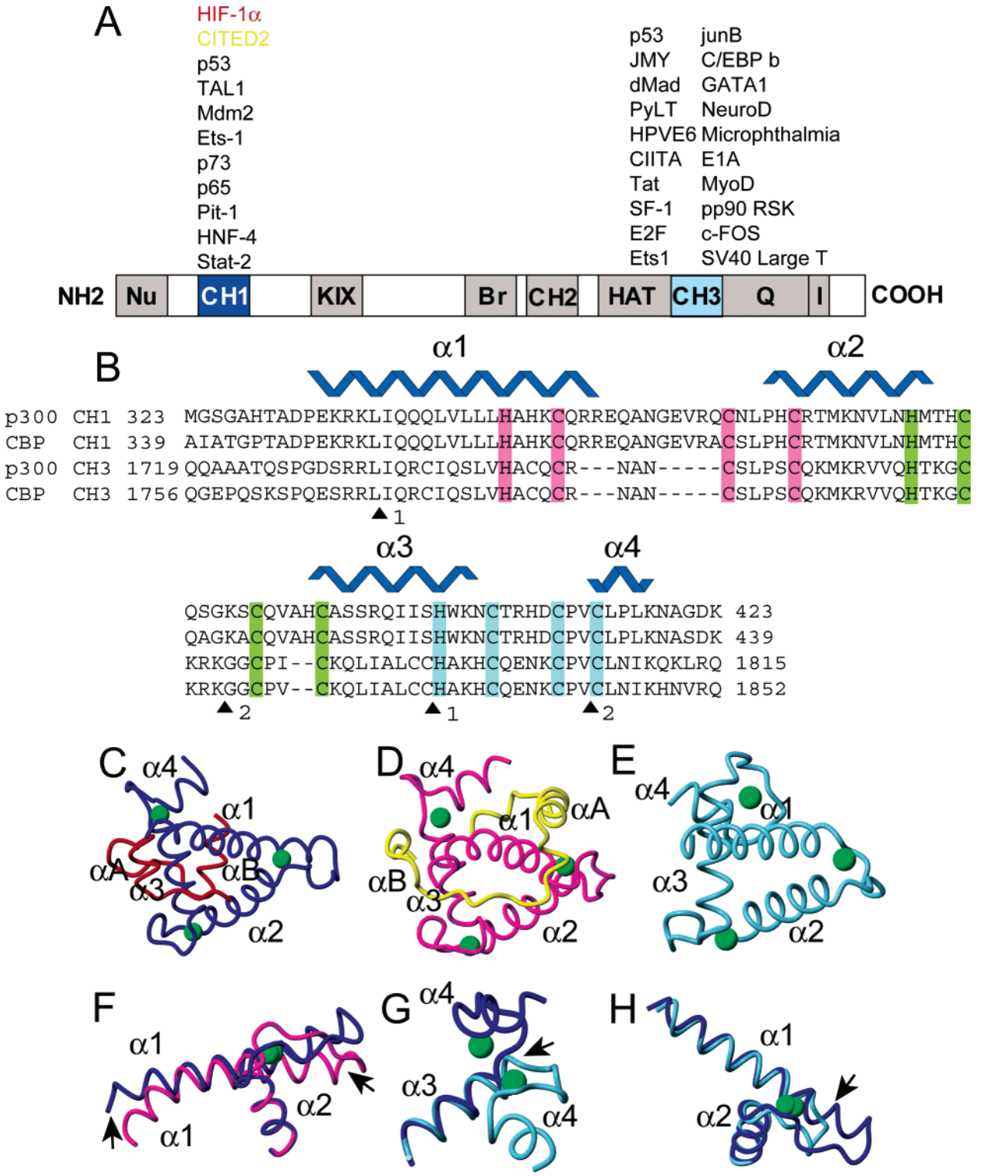

FIGURE 1: Domains of p300/CBP and CH1/CH3 sequences and structures. (A) Schematic representation of the p300/CBP domains from the N-terminus to the C-terminus. In order, these are nuclear hormone receptor-binding domain (Nu), CH1, CREB-binding domain (KIX), bromodomain (Br), CH2, histone acetyltransferase domain (HAT), CH3, glutamine-rich domain (Q), and interferon regulatory factor 3-binding domain (I). Lists of CH1- and CH3-binding transcription factors are shown. (B) Sequences of human p300 and CBP CH1 and CH3 are aligned. Helical regions of CH1 derived from the HIF-1α TAD−CH1 complex are shown in dark blue (*19*). Strictly conserved histidines and cysteines of the three HCCC Zn^{2+}-binding clusters are grouped according to color. The arrowheads indicate insertions in the CH3 sequences relative to the CH1 sequences, and the number of residues inserted is shown. (C) Structure of the HIF-1α TAD−p300 CH1 complex [PDB entry 1L3E (*19*)]. (D) Structure of the CITED2 TAD−p300 CH1 complex [PDB entry 1P4Q (*21*)]. (E) Structure of CH3 [PDB entry 1F81 (*26*)]. (F) Superimposition of CH1 domains from the HIF-1α−p300 complex and the CITED2−p300 complex indicating differences in the helix α1 and first Zn^{2+}-binding loop conformations. (G) Superimposition of CH1 from the HIF-1α−p300 complex and free CH3 indicating the differences in the third Zn^{2+}-binding loop and helix α4 conformations. (H) Same superimposition as in panel G indicating differences in the first Zn^{2+}-binding loop conformations due to an eight-residue insertion in the CH1 sequence. HIF-1α is colored red, CITED2 yellow, CH1 from the HIF-1α complex dark blue, CH1 from the CITED2 complex magenta, and CH3 light blue, and Zn^{2+} ions are colored green. Arrows point to regions of conformational differences between superimposed structures.

homologous to PHD fingers (*18*); its function in p300/CBP is not as well characterized as that of CH1 or CH3.

Recruitment of p300/CBP by HIF-1 is becoming a model system for understanding CH1 domain interactions (*11*, *19*−*21*). HIF-1 transcribes hypoxia-response genes, including vascular endothelial growth factor, erythropoietin, nitric oxide synthetase, and glycolytic enzymes, in response to a hypoxic stimulus (*22*). HIF-1 is heterodimeric and contains an oxygen-sensitive HIF-1α subunit and a constitutively expressed HIF-1*β* subunit. During hypoxia, HIF-1 recruits p300/CBP to promoters containing hypoxia-response elements through a high-affinity interaction between the HIF-1α transactivation domain and the p300/CBP CH1 domain (*11*, *19*, *20*). Binding to CH1 is prevented during normoxia by post-translational hydroxylation of Asn803 within the HIF-1α transactivation domain (*23*); this modification has the dual role of disrupting a helix in the HIF-1α transactivation domain and sterically interfering with binding to CH1 (*19*). In addition, hydroxylation of Pro402 and Pro564 targets HIF-1α for ubiquitin-mediated degradation by allowing it to interact with the von Hippel-Lindau protein (pVHL), a component of an E3 ubiquitin ligase complex (*24*, *25*). Interestingly, CITED2, a hypoxia-response gene product of HIF-1, can turn off HIF-1-mediated transcription by competing with HIF-1α for binding to the CH1 domain (*12*).

The structures of free CH3 and bound CH1 in complexes with the HIF-1α TAD and CITED2 TAD are known (*19*−*21*, *26*, *27*). Free CH3 and ligand-bound CH1 are structurally homologous as expected on the basis of sequence homology; each domain has three long helices that cross each other to form a compact globular fold (Figure 1). A fourth helix projects away from the core CH1−CH3 structure, but is oriented differently in each domain. Connecting the helices are three loops, each of which coordinates one Zn^{2+} ion through three cysteines and one histidine. The HIF-1α and CITED2 TADs interact with CH1 by wrapping around helix α3 and helix α1, respectively (*21*). Thus, one structural explanation for CH1's diverse binding properties is that it has more than one binding surface. The TAD binding surfaces on CH1 do, however, overlap, and therefore, competition for this common binding site is the structural basis for negative regulation of HIF-1α by CITED2 (*21*). Interestingly, helix α4 in CH3 occupies the same conformational space that the HIF-1α and CITED2 TADs occupy on CH1, thereby providing a potential structural explanation for CH1 specificity. However, the absence of a free CH1 structure precludes a firm conclusion about whether the helix α4 conformation is a true structural difference between CH1 and CH3 or whether it simply represents a ligand-induced conformational change in the former.

A current model for CH1 binding is that CH1 presents a stable structural scaffold for protein folding. Our group and others have demonstrated that transactivation domains from HIF-1α and CITED2 bind and fold on CH1 simultaneously (*19*, *21*). In this report, we describe the biophysical and structural properties of CH1 in the absence of a protein ligand and compare them to those of a HIF-1α TAD−p300 CH1 complex. We find that CH1 can exist in three different conformational states depending on whether it is metal-free, bound to Zn^{2+}, or bound to Zn^{2+} and HIF-1α. The functional implications of this three-state model for CH1 are discussed.

MATERIALS AND METHODS

Protein Preparation. The human HIF-1α TAD (786−826)−p300 CH1 (323−423) complex was expressed in *Escherichia coli* and purified using the GST−glutathione expression and purification system as described previously (*19*). A synthetic HIF-1α TAD peptide (790−826) was prepared using standard Fmoc chemistry on an Applied Biosystems 430A peptide synthesizer. Following cleavage, the peptide was purified by HPLC (Beckman, System Gold) over a C18 reverse-phase column (Vydac, 250 mm × 21.5 mm) using a linear gradient of acetonitrile and 0.1% trifluoroacetic acid. Alternatively, a recombinant HIF-1α TAD peptide (786−826) was obtained by separating the purified HIF-1α (786−826)−p300 (323−423) complex by reverse-phase HPLC. Elution fractions containing peptides were pooled and lyophilized for storage at −20 °C.

The CH1 domain (323−423) was expressed in *E. coli* strain BL21(DE3) using a pACYC plasmid. Typically, bacteria (1 L) were grown in LB medium at 37 °C to an optical density of 0.5−0.6 at 600 nm, and then induced with 1 mM IPTG for 3 h at the same temperature. Alternatively, bacteria were grown and induced in ^{15}N-containing minimal medium (Bio-Express, Cambridge Isotope Labs) to prepare isotope-labeled CH1 for NMR spectroscopy. Bacteria were harvested at 6000*g* for 20 min, washed with 50 mL of 20 mM Tris-HCl (pH 8.0), reharvested, and then frozen at −20 °C. The bacterial pellet was thawed at room temperature, resuspended in 50 mL of 20 mM Tris-HCl (pH 8.0), 0.1 mg/mL lysozyme, 1 mM dithiothreitol, 0.1 mM $ZnSO_4$, and one EDTA-free protease inhibitor tablet (Roche Molecular Biochemicals), and then sonicated. The soluble fraction was separated from inclusion bodies and other insoluble material by ultracentrifugation at 40 000 rpm for 30 min using a 70Ti rotor (Beckman). CH1 obtained from bacteria grown in LB was mostly soluble, whereas ^{15}N-labeled CH1 obtained from bacteria grown in minimal media was mostly insoluble; nutrient-enriched Bio-Express minimal medium (Cambridge Isotope Labs) improved the recovery of soluble ^{15}N-labeled CH1. The CH1 pI of 9.39 enabled separation from most *E. coli* proteins by cation exchange at pH 8.0. Thus, the soluble fraction of bacterial extract was filtered through a 0.2 *μ*m filter, then loaded through a superloop over a 1 mL HiTrap SP HP column (Amersham Biosciences) in 20 mM Tris-HCl (pH 8.0) and 0.1 mM $ZnSO_4$, and eluted in a continuous NaCl gradient using an ÄKTA purifier (Amersham Biosciences). The elution fractions containing CH1 were pooled and concentrated using a 15 mL ultrafree centrifugal filter device (Millipore), and then purified again over a Superdex 75 HR gel filtration column (Amersham Biosciences). The sample volume was reduced to 0.5 mL, and the final concentration was determined by absorbance at 280 nm (extinction coefficient of 5690 M^{-1} cm^{-1}). The purity and quality of the sample were assessed by SDS−PAGE. All CH1 samples contained Zn^{2+} ions unless they were removed intentionally by chelation with EDTA or by repurification using reverse-phase HPLC; a possible perturbation in pH because of the addition of EDTA was controlled with the buffers used as confirmed by measuring the pH of the samples.

CD Spectroscopy. CD spectra were recorded on an Aviv 62DS spectropolarimeter equipped with a thermoelectric temperature controller. CH1−Zn^{2+} and CH1−Zn^{2+}−HIF-

1α samples contained 5 μM protein (for a 1.0 cm cell) or 20 μM protein (for a 0.1 cm cell) in a buffer containing 20 mM MES (pH 6.0) and 100 mM NaCl, or 20 mM Tris-HCl (pH 8.0) and 100 mM NaCl. Metal-free CH1 was prepared by chelating Zn^{2+} ions with 5 mM EDTA. Far-UV and near-UV CD spectra represent the average of five scans measured at 25 °C using a step size of 1 nm and a signal averaging time of 3 s. Thermal denaturation was assessed at 222 nm between 25 and 80 °C in 2 °C increments with equilibration over 2 min and data acquisition over 30 s. All spectra were corrected for the baseline by subtracting control spectra of buffer alone. The following equation was used to convert raw data in mole degrees to molar ellipticity per residue: (mole degrees × 100)/(number of amino acids × path length × peptide concentration).

Fluorescence Spectroscopy. Spectra were recorded on an SLM 8000C fluorescence spectrometer at 25 °C using a 1 cm path length cuvette and 4 nm excitation and 4 nm emission slit widths. Following excitation at 280 or 295 nm, baseline emission spectra of 2 μM metal-free CH1, CH1−Zn^{2+}, or CH1−Zn^{2+}−HIF-1α in 20 mM MES (pH 6.0) or in 20 mM Tris-HCl (pH 8.0), 100 mM NaCl, and 0.1 mM $ZnSO_4$ were recorded from 200 to 400 nm at intervals of 1 nm/s.

For ANS binding experiments, baseline emission spectra of 2 μM ANS (Molecular Probes) in 20 mM MES (pH 6.0) or in 20 mM Tris-HCl (pH 8.0), 100 mM NaCl, and 0.1 mM $ZnSO_4$ were recorded between 375 and 650 nm at intervals of 1 nm/s following excitation at 370 nm. Following the addition of metal-free CH1, CH1−Zn^{2+}, or CH1−Zn^{2+}−HIF-1α to a final concentration of 2 μM, ANS emission spectra were acquired again and compared to those for ANS alone.

For Zn^{2+} binding experiments, samples contained 1 μM metal-free CH1, 20 mM MES (pH 6.0), and 100 mM NaCl. Metal-free CH1 was prepared by chelating Zn^{2+} from CH1 with EDTA (2 mM), and then repurifying metal-free CH1 by gel filtration (Superdex 75 HR) in 20 mM MES (pH 6.0) and 100 mM NaCl pretreated with Chelex beads (Bio-Rad) to remove ambient levels of Zn^{2+} ions. Samples were excited at 280 nm, and fluorescence emission was measured at 335 nm. Samples were allowed to equilibrate for 5 min following each titration, and then fluorescence data points were recorded at 1 s intervals for 100 s. EDTA (2 mM) was added at the end of Zn^{2+} titration to assess reversibility. Zn^{2+} binding spectra were corrected for buffer dilution effects by subtracting spectra obtained with buffer alone.

For HIF-1α binding experiments, samples contained 1 μM CH1−Zn^{2+}, 50 mM Tris-HCl (pH 8.0) or 20 mM MES (pH 6.0), and 100 mM NaCl. Samples were excited at 280 nm, and fluorescence emission was measured at 335 nm. Samples were allowed to equilibrate for 5 min following each titration, and then fluorescence data points were recorded at $^1/_{10}$ s intervals for 5 s. HIF-1α binding spectra were corrected for dilution and HIF-1α peptide effects by subtracting spectra obtained by HIF-1α titration in the presence of 2 mM EDTA. The final fluorescence for both Zn^{2+} and HIF-1α binding experiments is reported as $[(F_1 - F_0)/F_1] \times 100$, where F_0 is the initial fluorescence and F_1 the final fluorescence. Each data point represents the average value for all data points collected at each ligand concentration.

NMR Spectroscopy. All $^1H-^{15}N$ HSQC spectra were acquired at 25 °C on a Bruker Avance 500 or 600 MHz spectrometer equipped with cryogenic probes. A sample containing 100 μM ^{15}N-labeled CH1, 5 mM deuterated MES (pH 6.0), 100 mM NaCl, 0.1 mM $ZnSO_4$, and 10.0% (v/v) D_2O was prepared by buffer exchange over a PD10 column (Amersham Biosciences). Addition of unlabeled HIF-1α peptide (790−826) to a final concentration of 250 μM was used to assess formation of a CH1−Zn^{2+}−HIF-1α complex. Metal-free CH1 was prepared by addition of 2 mM EDTA to [^{15}N]CH1−Zn^{2+}. NMR processing and analysis were carried out using PROSA (*28*) and XEASY (*29*). Structures in Figure 1 were prepared using the graphics display program MOLMOL (*30*, *44*).

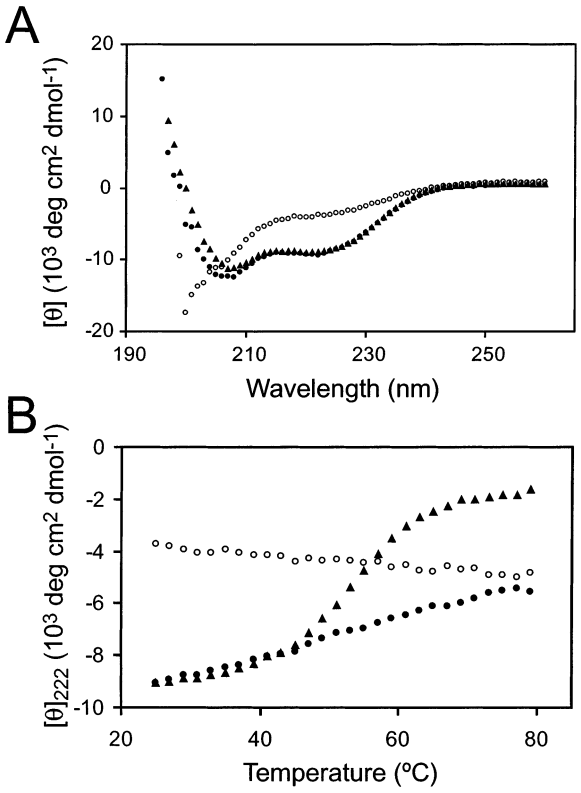

FIGURE 2: Far-UV CD spectra and thermal denaturation of CH1. (A) CD spectra of CH1−Zn^{2+} (●) and CH1−Zn^{2+}−HIF-1α (▲) show similar helical patterns characterized by negative deflections at 222 and 209 nm. In contrast, metal-free CH1 (○) is mostly random coil. (B) The thermal unfolding of CH1−Zn^{2+} (●) as a function of molar ellipticity per residue at 222 nm is linear, whereas unfolding of CH1−Zn^{2+}−HIF-1α (▲) is cooperative. Metal-free CH1 (○) has negligible ellipticity at this wavelength and is mostly unfolded at the starting temperature (25 °C).

RESULTS

The far-UV CD spectrum of CH1−Zn^{2+} shows that the major secondary structure is helical as for the CH1−Zn^{2+}−HIF-1α complex (Figure 2A). Spectra of CH1−Zn^{2+} in 100 mM NaCl at pH 6 and 8 were the same (data not shown); therefore, all further experiments were performed at either pH value or at both values. The thermal stability of CH1−Zn^{2+} helical structure between 25 and 80 °C was monitored by changes in ellipticity at 222 nm (Figure 2B). Unexpectedly, the melting curve shows noncooperative, reversible unfolding, which is characteristic of molten globule proteins. This result differs from the cooperative, unfolding pattern of the CH1−Zn^{2+}−HIF-1α complex as reported by us previously (*21*) and reproduced again here. The CD spectrum

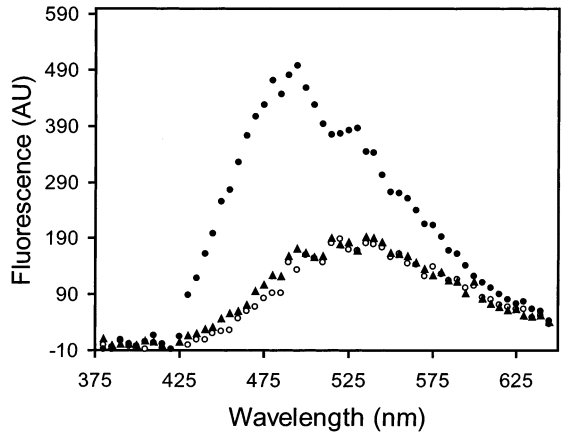

FIGURE 3: ANS binding to CH1. Fluorescence emission spectra of ANS alone (○), ANS with CH1−Zn^{2+} (●), and ANS with CH1−Zn^{2+}−HIF-1α (▲). ANS binds CH1−Zn^{2+} but does not bind CH1−Zn^{2+}−HIF-1α.

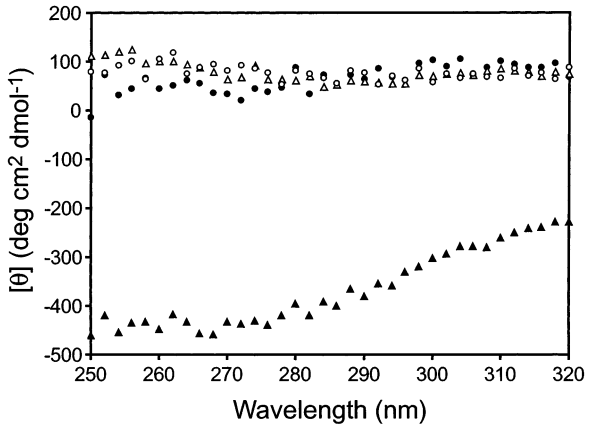

FIGURE 4: Near-UV CD spectra of CH1. The CD spectrum of CH1−Zn^{2+}−HIF-1α (▲) has a near-UV signal, whereas the spectra of CH1−Zn^{2+} (●), metal-free CH1 (○), and a CH1−Zn^{2+}−HIF-1α complex disrupted by EDTA (△) do not exhibit any emission changes in this region.

of metal-free CH1 exhibits a marked loss of helical structure, and no significant change in ellipticity at 222 nm when heated to the maximal temperature (Figure 2).

On the basis of the results presented above, we performed additional experiments to characterize the molten globule features of CH1−Zn^{2+}, and then compare them to the structural features of CH1−Zn^{2+}−HIF-1α. The hydrophobic fluorophore, ANS, characteristically binds molten globule proteins because their hydrophobic interiors are open and accessible, but does not bind compact, well-ordered globular structures whose hydrophobic cores are protected from solvent. We found that addition of CH1−Zn^{2+} to ANS enhanced the ANS fluorescence emission spectrum and was therefore consistent with ANS binding (Figure 3). Metal-free CH1 also bound ANS (data not shown). In contrast, addition of CH1−Zn^{2+}−HIF-1α at the same concentration did not perturb the ANS emission spectrum. Another classical feature of molten globule proteins is the absence of a near-UV elliptical signal. Neither CH1−Zn^{2+} nor metal-free CH1 exhibits an elliptical signal in the near-UV range (Figure 4). In contrast, CH1−Zn^{2+}−HIF-1α did have a weak signal. Disruption of this complex by removing Zn^{2+} ions with EDTA caused the loss of this absorption signal.

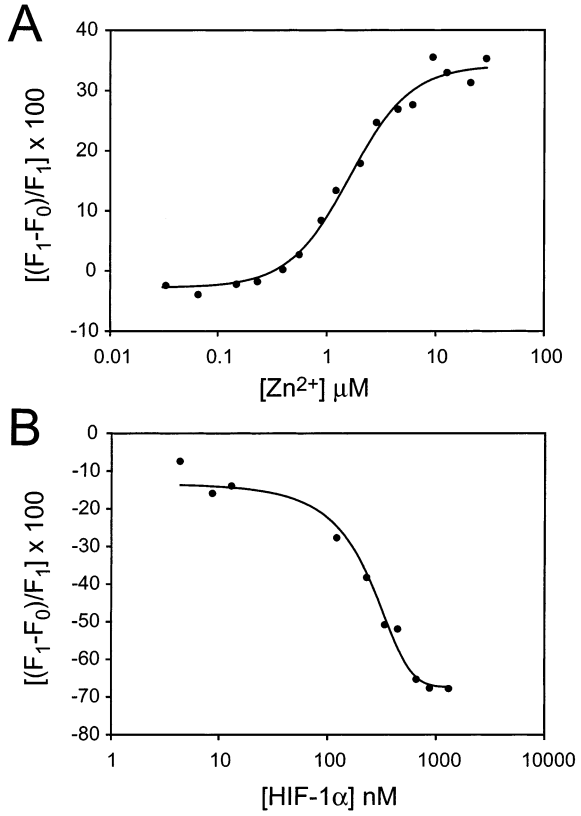

FIGURE 5: Conformational changes upon Zn^{2+} and HIF-1α TAD binding to CH1. (A) Fluorescence change of metal-free CH1 as a function of increasing Zn^{2+} concentration. (B) Fluorescence change of CH1−Zn^{2+} as a function of increasing HIF-1α TAD peptide concentration.

The CH1 domain binds three Zn^{2+} ions as determined by electrospray mass spectrometry and by the structural organization of Zn^{2+}-binding residues into three discrete coordination centers in the CH1−Zn^{2+}−HIF-1α structure (*19*, *20*). A Zn^{2+} binding experiment was performed to measure the average binding affinity for Zn^{2+} ions. Tryptophan 403 in CH1 is the only fluorophore, and therefore provides an intrinsic probe for monitoring conformational changes associated with Zn^{2+} binding. Excitation of CH1−Zn^{2+} at 280 nm has a wavelength of maximal emission (λ_{max}) of 338 nm; in contrast, the λ_{max} for CH1 when Zn^{2+} ions are removed with EDTA is 349 nm and relatively quenched, and the λ_{max} for CH1−Zn^{2+}−HIF-1α is 328 nm (data not shown). The red shift of λ_{max} for metal-free CH1 and the blue shift of λ_{max} for CH1−Zn^{2+}−HIF-1α are consistent with a less folded state and more folded state, respectively, compared to CH1−Zn^{2+}. Titration of metal-free CH1 (prepared without EDTA present) with Zn^{2+} resulted in a sigmoidal pattern of fluorescence enhancement (Figure 5A). The EC_{50} value is 1.6 μM. As expected, the addition of EDTA reversed the fluorescence change to baseline. Also as expected, addition of excess Zn^{2+} to CH1−Zn^{2+} in a Zn^{2+}-free solvent had no effect on fluorescence. Thus, Zn^{2+} binding is associated with a conformational change in CH1 as detected by intrinsic tryptophan fluorescence.

The CH1 and HIF-1α peptides can be coexpressed in bacteria and purified as a complex. Next, we determined whether this complex could be reconstituted from purified peptides. Binding of the HIF-1α peptide (residues 786−826)

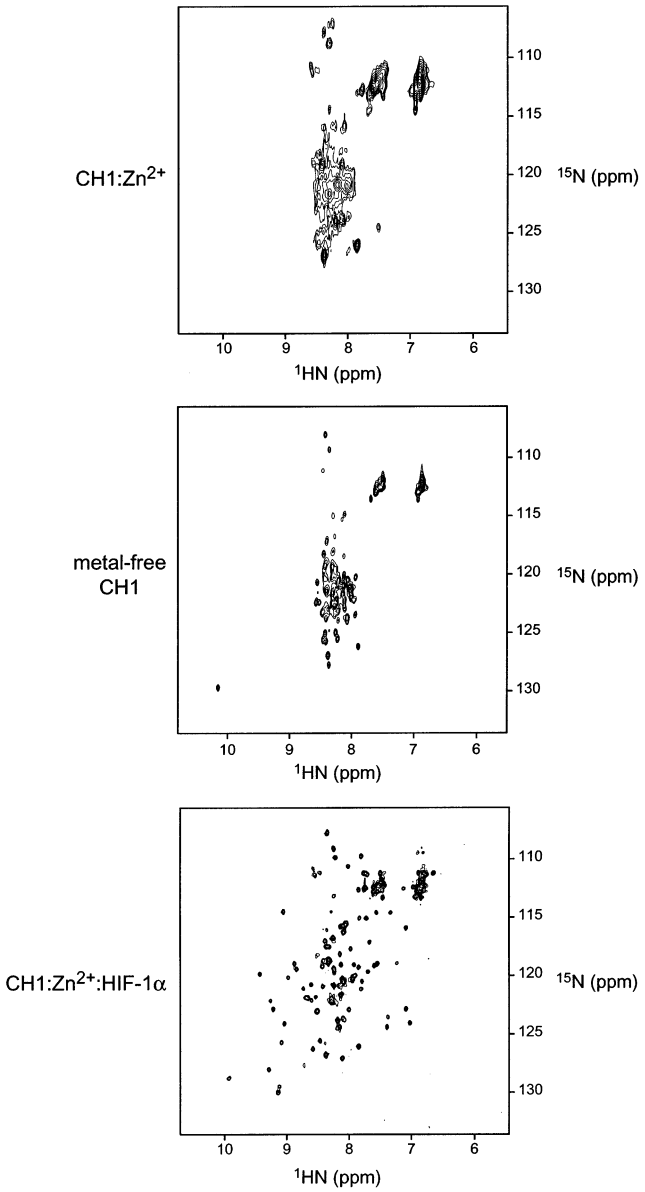

FIGURE 6: NMR $^1H-^{15}N$ HSQC spectra of CH1: (top) CH1−Zn^{2+}, (middle) metal-free CH1, and (bottom) CH1−Zn^{2+}−HIF-1α. Note that the CH1−Zn^{2+} spectrum exhibits only a few poorly dispersed cross-peaks which are broad; that of metal-free CH1 shows more poorly dispersed cross-peaks with narrower line widths, and that of CH1−Zn^{2+}−HIF-1α has many dispersed cross-peaks with narrow line widths. Each spectrum, therefore, represents a different CH1 structure.

to CH1−Zn^{2+} was monitored by fluorescence spectroscopy (Figure 5B). Addition of the HIF-1α peptide caused a fluorescence decrease that plateaued in the low micromolar range, and had an EC_{50} value of 200 nM. In contrast, no fluorescence change was detected when the HIF-1α peptide was added to metal-free CH1 (i.e., in the presence of excess EDTA). Thus, binding of HIF-1α to CH1 induces a second conformational change in CH1.

The $^1H-^{15}N$ HSQC spectrum of a protein provides a "fingerprint" of its structure because the chemical environment of each residue affects its backbone amide proton and nitrogen chemical shift values. The spectrum of Zn^{2+}-bound CH1 is shown in Figure 6. There are fewer than expected cross-peaks present, and they have extremely broad line widths. The broad peaks are likely the result of chemical exchange phenomena among many conformational states; protein aggregation is excluded by the monomeric size of CH1 estimated by gel filtration (data not shown). Thus, these NMR data are consistent with CH1 as a molten globule (*31*). Addition of EDTA to remove Zn^{2+} ions produces more cross-peaks with sharper line widths. All amide protons are centered around the random coil value of 8.35 ppm, consistent with a completely unfolded molecule. Addition of a 2.5-fold molar excess of unlabeled HIF-1α peptide (790−826) to the CH1−Zn^{2+} protein produced a marked increase in the number of cross-peaks having narrow line widths. Moreover, the dispersion of these cross-peaks indicates a well-ordered structure. The cross-peak pattern is nearly identical to that of a HIF-1α TAD−CH1 complex coexpressed in bacteria and purified as a complex (*19*). The removal of metal ions from CH1 precludes HIF-1α TAD from binding.

DISCUSSION

This study demonstrates different conformational states for metal-free CH1, Zn^{2+}-bound CH1, and the HIF-1α−CH1 complex. CH1−Zn^{2+} has significant helical secondary structure, but lacks well-defined tertiary structure. In contrast, metal-free CH1 is almost completely disordered, and CH1 in complex with the HIF-1α TAD is stable and completely ordered. It is unlikely that bacteria misfold free CH1−Zn^{2+} because the same bacteria produce correctly folded complexes between CH1 and HIF-1α or CITED2 TADs (*19*, *21*), and as shown here, free CH1−Zn^{2+} can bind a HIF-1α TAD peptide to saturation. In fact, when CH1 is denatured by HPLC purification in acetonitrile and then refolded with Zn^{2+} under different conditions, the refolded CH1−Zn^{2+} has different structural and functional properties compared to CH1−Zn^{2+} purified from bacteria. The $^1H-^{15}N$ HSQC spectrum of refolded CH1−Zn^{2+} shows a small population of weak cross-peaks, which appear like the bacterially produced form, but a major population of strong cross-peaks with narrow line widths and intermediate dispersion (relative to the unfolded form and the form in complex with HIF-1α), suggestive of a misfolded protein (data not shown). Moreover, only a small fraction of this refolded protein can bind the HIF-1α TAD peptide in contrast to fully functional, bacterially produced CH1−Zn^{2+}.

Previous work suggested that metal-free CH1 was disordered on the basis of the absence of NMR chemical shift dispersion when a complex of CH1 and HIF-1α were disrupted with EDTA (*19*). However, no other structural or biophysical information was available for full-length metal-free or Zn^{2+}-bound CH1. In a study by Newton et al., a 27-residue Zn^{2+}-bound CH1 peptide (CBP residues 376−402) had some helical content on the basis of CD and H^α proton chemical shift index data (*32*). This region corresponds to helix α2 in the HIF-1α−CH1 complex structures (*19*, *20*). The ends of the peptide contain partial HCCC Zn^{2+}-binding motifs for two Zn^{2+} ions (i.e., the two C-terminal cysteines from Zn^{2+}-binding site 1 and the N-terminal histidine and cysteine from Zn^{2+}-binding site 2). The three-dimensional structure of this peptide was determined by NMR spectroscopy, and shows two short helices connected by a loop (*33*). The tertiary structure is defined by coordination of a single Zn^{2+} ion. The authors acknowledge that this structure represents a nonphysiologically active form due to the variant

Zn^{2+}-binding motif (CCHC instead of native HCCC), and have termed it a CHANCE finger (cysteine/histidine exhibiting a nonexpected conformational ensemble). Nonetheless, this fold proved to be stable to thermal denaturation and multiple alanine substitutions. These structural and biophysical attributes differ substantially from those of full-length CH1−Zn^{2+} determined here.

A molten globule is defined as a partially folded structural intermediate (*34*−*36*). As such, molten globules have native-like secondary structure but are devoid of the fixed packing interactions that define a stable tertiary structure. α-Lactalbumin (αLA) has served as a model in studying the molten globule state (*37*). αLA forms a molten globule under denaturing conditions (e.g., low pH) or in the absence of Ca^{2+} ions. Several criteria have been put forth to classify the molten globule state (*38*), many of which belong to the Zn^{2+}-bound CH1 domain. (1) The secondary structure content determined by far-UV CD spectroscopy is similar in the molten globule and folded states. (2) The environments of the side chains determined by near-UV CD spectroscopy and NMR spectroscopy are homogeneous for the molten globule state and asymmetric for the folded state. (3) Unfolding of the molten globule state is rapid and noncooperative, whereas unfolding of the folded state is slow and cooperative. (4) The solvent-exposed hydrophobic core of molten globules binds the hydrophobic fluorophore ANS, whereas the fully folded form cannot do the same. Unfortunately, the absence of stable tertiary structure and conformational heterogeneity has precluded high-resolution structure determination of molten globule proteins. The molten globule state of αLA produces very few $^{1}H-^{15}N$ cross-peaks by NMR spectroscopy (*31*). This result is attributed to extreme broadening of cross-peaks as a result of conformational fluctuation on a millisecond time scale (*39*). We found similar results for CH1−Zn^{2+} whereby there were fewer and broader cross-peaks than in the fully folded form (in complex with HIF-1α) or unfolded metal-free form. The visible cross-peaks of CH1−Zn^{2+} are poorly dispersed; most likely, cross-peaks belonging to residues in partially folded regions are more dispersed but too broad to be observed.

The results presented here for Zn^{2+}-bound CH1 are in stark contrast to those reported by De Guzman et al. for Zn^{2+}-bound CH3 (*26*). The $^{1}H-^{15}N$ HSQC spectrum of CH3−Zn^{2+} looks all together different from that for CH1−Zn^{2+}; there are numerous, well-dispersed peaks with narrow line widths for CH3−Zn^{2+} (*26*). Consequently, CH3−Zn^{2+} has well-defined secondary and tertiary structures. These dramatic differences between free CH1−Zn^{2+} and CH3−Zn^{2+} structures are surprising given that CH1 in complexes with HIF-1α or CITED2 TADs is structurally homologous to free CH3−Zn^{2+} (i.e., rmsd of 1.0 Å) (*19*). However, chimeras between different species of αLA, and even single-amino acid substitutions in αLA, can help stabilize the molten globule state (*40*, *41*). Therefore, subtle sequence differences between CH1 and CH3 may have pronounced effects on the structural stability of this Zn^{2+}-binding module. We also speculate that differences in the Zn^{2+}-binding sites between CH1 and CH3 may be responsible for their structural differences. For instance, the first Zn^{2+}-binding site in CH1 has an eight-amino acid insertion between the second and third cysteines of the HCCC motif. As a result, the structure of the first Zn^{2+}-binding loop is different for free CH3 and bound CH1 in complex with HIF-1α and CITED2 TADs (Figure 1). In free CH1−Zn^{2+}, this insertion may destabilize the first Zn^{2+}-binding site until CH1 binds a transcription factor ligand. The conformational differences between the first Zn^{2+}-binding loop in the HIF-1α−CH1 complex and CITED2−CH1 complex are consistent with the notion of a flexible first Zn^{2+}-binding loop (Figure 1).

What is the biological importance of this three-state model of CH1? Metal-free CH1 does not bind transcription factor TADs (*19*, *21*). Thus, the accessibility to Zn^{2+} ions within the cell will determine if p300/CBP can interact with certain transcription factors. Transcription factor TADs derived from HIF-1α and CITED2 are unstructured until they bind CH1 and fold. A current model for CH1 protein interactions is one in which CH1 provides a versatile scaffold for protein folding, thereby implying that Zn^{2+}-bound CH1 has a rigid structure. In fact, this model should now be modified to incorporate the current structural information indicating that Zn^{2+}-bound CH1 is only partially folded. It thus appears that CH1 and its transcription factor ligands *cofold* to produce a compact, stable complex structure. Cofolding was also observed between the p160 nuclear-receptor coactivator and a C-terminal domain of CBP, which the authors of this report termed "mutual synergistic folding" (*42*). More generally, folding as a means of binding is becoming an increasingly common theme in protein−protein interactions, and provides a mechanism by which one structural domain can interact with multiple partners (*43*). Part of this versatility in protein−protein interaction is a product of the structural plasticity inherent in a folding model for binding. For instance, the crossing angles of helix α1 with respect to the rest of the CH1 structure differ between the HIF-1α−CH1 and CITED2−CH1 complex structures (Figure 1). This plasticity of CH1 is necessary to accommodate binding to either HIF-1α or CITED2 without steric interference; rigid body interactions would not be quite as tolerant. In addition, the helix α4 conformational differences between ligand-bound CH1 and free CH3 may not impart structural specificity for transcription factor binding as initially suggested (*19*, *21*), but instead represent a ligand-induced change upon cofolding. Another advantage of cofolding is that each protein in the complex can present large internal hydrophobic surfaces for enhanced binding affinity. Indeed, both the HIF-1α TAD−CH1 and CITED2 TAD−CH1 complexes have extensive intermolecular surfaces larger than most protein−protein interactions and have binding affinities in the low nanomolar range (*19*, *21*). Consequently, these complexes appear like single structural domains (Figure 1).

In conclusion, the p300 CH1 domain can assume three conformational states depending on Zn^{2+} ion and transcription factor binding. The characterization of Zn^{2+}-bound CH1 as a partially folded molecule with molten globule features is a novel, unexpected finding. These results add substantially to our understanding of how p300/CBP functions as an adaptor between numerous transcription factors and the basal transcriptional machinery.

ACKNOWLEDGMENT

We thank S. Blacklow for helpful suggestions and use of his CD spectrometer, G. Wagner for use of his NMR spectrometers, M. Jacobs for synthesizing the HIF-1α TAD

peptide, and F. Poy, M. Eck, and A. Kung for sharing plasmid constructs.

REFERENCES

1. Vo, N., and Goodman, R. H. (2001) CREB-binding protein and p300 in transcriptional regulation, *J. Biol. Chem. 276*, 13505−13508.
2. Grossman, S. R., Deato, M. E., Brignone, C., Chan, H. M., Kung, A. L., Tagami, H., Nakatani, Y., and Livingston, D. M. (2003) Polyubiquitination of p53 by a ubiquitin ligase activity of p300, *Science 300*, 342−344.
3. Giles, R. H., Peters, D. J., and Breuning, M. H. (1998) Conjunction dysfunction: CBP/p300 in human disease, *Trends Genet. 14*, 178−183.
4. Goodman, R. H., and Smolik, S. (2000) CBP/p300 in cell growth, transformation, and development, *Genes Dev. 14*, 1553−1577.
5. Petrij, F., Giles, R. H., Dauwerse, H. G., Saris, J. J., Hennekam, R. C., Masuno, M., Tommerup, N., van Ommen, G. J., Goodman, R. H., Peters, D. J., et al. (1995) Rubinstein-Taybi syndrome caused by mutations in the transcriptional co-activator CBP, *Nature 376*, 348−351.
6. Borrow, J., Stanton, V. P., Jr., Andresen, J. M., Becher, R., Behm, F. G., Chaganti, R. S., Civin, C. I., Disteche, C., Dube, I., Frischauf, A. M., Horsman, D., Mitelman, F., Volinia, S., Watmore, A. E., and Housman, D. E. (1996) The translocation t(8;16)(p11;p13) of acute myeloid leukaemia fuses a putative acetyltransferase to the CREB-binding protein, *Nat. Genet. 14*, 33−41.
7. Eckner, R., Ewen, M. E., Newsome, D., Gerdes, M., DeCaprio, J. A., Lawrence, J. B., and Livingston, D. M. (1994) Molecular cloning and functional analysis of the adenovirus E1A-associated 300-kD protein (p300) reveals a protein with properties of a transcriptional adaptor, *Genes Dev. 8*, 869−884.
8. Arany, Z., Sellers, W. R., Livingston, D. M., and Eckner, R. (1994) E1A-associated p300 and CREB-associated CBP belong to a conserved family of coactivators, *Cell 77*, 799−800.
9. Arany, Z., Newsome, D., Oldread, E., Livingston, D. M., and Eckner, R. (1995) A family of transcriptional adaptor proteins targeted by the E1A oncoprotein, *Nature 374*, 81−84.
10. Ponting, C. P., Blake, D. J., Davies, K. E., Kendrick-Jones, J., and Winder, S. J. (1996) ZZ and TAZ: new putative zinc fingers in dystrophin and other proteins, *Trends Biochem. Sci. 21*, 11−13.
11. Kung, A. L., Wang, S., Klco, J. M., Kaelin, W. G., and Livingston, D. M. (2000) Suppression of tumor growth through disruption of hypoxia-inducible transcription, *Nat. Med. 6*, 1335−1340.
12. Bhattacharya, S., Michels, C. L., Leung, M. K., Arany, Z. P., Kung, A. L., and Livingston, D. M. (1999) Functional role of p35srj, a novel p300/CBP binding protein, during transactivation by HIF-1, *Genes Dev. 13*, 64−75.
13. Bhattacharya, S., Eckner, R., Grossman, S., Oldread, E., Arany, Z., D'Andrea, A., and Livingston, D. M. (1996) Cooperation of Stat2 and p300/CBP in signalling induced by interferon-alpha, *Nature 383*, 344−347.
14. Grossman, S. R., Perez, M., Kung, A. L., Joseph, M., Mansur, C., Xiao, Z. X., Kumar, S., Howley, P. M., and Livingston, D. M. (1998) p300/MDM2 complexes participate in MDM2-mediated p53 degradation, *Mol. Cell 2*, 405−415.
15. Gerritsen, M. E., Williams, A. J., Neish, A. S., Moore, S., Shi, Y., and Collins, T. (1997) CREB-binding protein/p300 are transcriptional coactivators of p65, *Proc. Natl. Acad. Sci. U.S.A. 94*, 2927−2932.
16. Yang, C., Shapiro, L. H., Rivera, M., Kumar, A., and Brindle, P. K. (1998) A role for CREB binding protein and p300 transcriptional coactivators in Ets-1 transactivation functions, *Mol. Cell. Biol. 18*, 2218−2229.
17. Grossman, S. R. (2001) p300/CBP/p53 interaction and regulation of the p53 response, *Eur. J. Biochem. 268*, 2773−2778.
18. Aasland, R., Gibson, T. J., and Stewart, A. F. (1995) The PHD finger: implications for chromatin-mediated transcriptional regulation, *Trends Biochem. Sci. 20*, 56−59.
19. Freedman, S. J., Sun, Z. Y., Poy, F., Kung, A. L., Livingston, D. M., Wagner, G., and Eck, M. J. (2002) Structural basis for recruitment of CBP/p300 by hypoxia-inducible factor-1 alpha, *Proc. Natl. Acad. Sci. U.S.A. 99*, 5367−5372.
20. Dames, S. A., Martinez-Yamout, M., De Guzman, R. N., Dyson, H. J., and Wright, P. E. (2002) Structural basis for Hif-1 alpha/CBP recognition in the cellular hypoxic response, *Proc. Natl. Acad. Sci. U.S.A. 99*, 5271−5276.
21. Freedman, S. J., Sun, Z. Y., Kung, A. L., France, D. S., Wagner, G., and Eck, M. J. (2003) Structural basis for negative regulation of hypoxia-inducible factor-1alpha by CITED2, *Nat. Struct. Biol. 10*, 504−512.
22. Semenza, G. L. (1999) Regulation of mammalian O_2 homeostasis by hypoxia-inducible factor 1, *Annu. Rev. Cell Dev. Biol. 15*, 551−578.
23. Lando, D., Peet, D. J., Whelan, D. A., Gorman, J. J., and Whitelaw, M. L. (2002) Asparagine hydroxylation of the HIF transactivation domain: a hypoxic switch, *Science 295*, 858−861.
24. Ivan, M., Kondo, K., Yang, H., Kim, W., Valiando, J., Ohh, M., Salic, A., Asara, J. M., Lane, W. S., and Kaelin, W. G., Jr. (2001) HIFalpha targeted for VHL-mediated destruction by proline hydroxylation: implications for O_2 sensing, *Science 292*, 464−468.
25. Jaakkola, P., Mole, D. R., Tian, Y. M., Wilson, M. I., Gielbert, J., Gaskell, S. J., Kriegsheim, A., Hebestreit, H. F., Mukherji, M., Schofield, C. J., Maxwell, P. H., Pugh, C. W., and Ratcliffe, P. J. (2001) Targeting of HIF-alpha to the von Hippel-Lindau ubiquitylation complex by O_2-regulated prolyl hydroxylation, *Science 292*, 468−472.
26. De Guzman, R. N., Liu, H. Y., Martinez-Yamout, M., Dyson, H. J., and Wright, P. E. (2000) Solution structure of the TAZ2 (CH3) domain of the transcriptional adaptor protein CBP, *J. Mol. Biol. 303*, 243−253.
27. Semenza, G. L. (2002) Physiology meets biophysics: visualizing the interaction of hypoxia-inducible factor 1 alpha with p300 and CBP, *Proc. Natl. Acad. Sci. U.S.A. 99*, 11570−11572.
28. Guntert, P., Dotsch, V., Wider, G., and Wuthrich, K. (1992) Processing of multidimensional NMR data with the new software PROSA, *J. Biomol. NMR 2*, 619−629.
29. Bartels, C., Xia, T.-H., Billeter, M., Guntert, P., and Wuthrich, K. (1995) The program XEASY for computer-supported NMR spectral analysis of biological macromolecules, *J. Biomol. NMR 5*, 1−10.
30. Koradi, R., Billeter, M., and Wuthrich, K. (1996) MOLMOL: a program for display and analysis of macromolecular structures, *J. Mol. Graphics 14*, 51−55.
31. Schulman, B. A., Kim, P. S., Dobson, C. M., and Redfield, C. (1997) A residue-specific NMR view of the non-cooperative unfolding of a molten globule, *Nat. Struct. Biol. 4*, 630−634.
32. Newton, A. L., Sharpe, B. K., Kwan, A., Mackay, J. P., and Crossley, M. (2000) The transactivation domain within cysteine/histidine-rich region 1 of CBP comprises two novel zinc-binding modules, *J. Biol. Chem. 275*, 15128−15134.
33. Sharpe, B. K., Matthews, J. M., Kwan, A. H., Newton, A., Gell, D. A., Crossley, M., and Mackay, J. P. (2002) A new zinc binding fold underlines the versatility of zinc binding modules in protein evolution, *Structure (London) 10*, 639−648.
34. Dobson, C. M. (1994) Protein folding. Solid evidence for molten globules, *Curr. Biol. 4*, 636−640.
35. Ptitsyn, O. B. (1995) Molten globule and protein folding, *Adv. Protein Chem. 47*, 83−229.
36. Creighton, T. E. (1997) How important is the molten globule for correct protein folding? *Trends Biochem. Sci. 22*, 6−10.
37. Kuwajima, K. (1996) The molten globule state of alpha-lactalbumin, *FASEB J. 10*, 102−109.
38. Creighton, T. E. (1993) *Proteins: Structure and Molecular Properties*, 2nd ed., W. H. Freeman and Co., New York.
39. Baum, J., Dobson, C. M., Evans, P. A., and Hanley, C. (1989) Characterization of a partly folded protein by NMR methods: studies on the molten globule state of guinea pig α-lactalbumin, *Biochemistry 28*, 7−13.
40. Mizuguchi, M., Masaki, K., Demura, M., and Nitta, K. (2000) Local and long-range interactions in the molten globule state: A study of chimeric proteins of bovine and human alpha-lactalbumin, *J. Mol. Biol. 298*, 985−995.
41. Uchiyama, H., Perez-Prat, E. M., Watanabe, K., Kumagai, I., and Kuwajima, K. (1995) Effects of amino acid substitutions in the hydrophobic core of alpha-lactalbumin on the stability of the molten globule state, *Protein Eng. 8*, 1153−1161.
42. Demarest, S. J., Martinez-Yamout, M., Chung, J., Chen, H., Xu, W., Dyson, H. J., Evans, R. M., and Wright, P. E. (2002) Mutual

synergistic folding in recruitment of CBP/p300 by p160 nuclear receptor coactivators, *Nature 415*, 549−553.
43. Dyson, H. J., and Wright, P. E. (2002) Coupling of folding and binding for unstructured proteins, *Curr. Opin. Struct. Biol. 12*, 54−60.
44. Koradi, R., Billeter, M., and Wuthrich, K. (1996) MOLMOL: a program for display and analysis of macromolecular structures, *J. Mol. Graphics 14*, 29−32.

BI034989O